A Specialized Thermal-hydraulic Code with Porous Media Model and SIMPLEC Algorithm for PB-FHRs

Yanzhi E, Yang Zou, and Hongjie Xu*
Shanghai Institute of Applied Physics, Chinese Academy of Sciences
Jialuo Road 2019, Shanghai, 201800, China
eyanzhi@sinap.ac.cn; zouyang@sinap.ac.cn; xuhongjie@sinap.ac.cn

Shixiong Song
Shanghai Institute of Applied Physics, Chinese Academy of Sciences
Jialuo Road 2019, Shanghai, 201800, China
songshixiong@sinap.ac.cn

Jie Zhang
Shanghai Institute of Applied Physics, Chinese Academy of Sciences
Jialuo Road 2019, Shanghai, 201800, China
songshixiong@sinap.ac.cn

ABSTRACT

Pebble bed fluoride-salt cooled high temperature reactors (PB-FHRs) are Generation IV reactors which use coated particle pebble fuels and liquid fluoride-salt coolants. Thermal-hydraulics analysis of reactor core is significant for both design and safety issues. A specialized code for core thermal-hydraulics analysis is very important for this novel reactor, which is also needed in detailed transient analysis. Aim of this study is to develop a thermal-hydraulic code (named GATH) based on CFD method for PB-FHRs to analyze thermal-hydraulic phenomena in reactor core. Porous media model is applied to simplify reactor geometry. Energy equations for solid region and fluid region are constructed respectively with considering local thermal non-equilibrium effect between fuels and coolants. Macroscopic mass and momentum equations are solved to get speed distribution and pressure drop of liquid by using SIMPLEC algorithm. The thermal dispersion mechanism in the pebble bed is considered by solving modified macroscopic turbulence equations with additional source terms. Empirical correlations are used to calculate effective heat conductivity of pebble bed, resistance terms and heat transfer coefficient. A simplified PB-FHR model is analyzed by GATH. The results indicate that the resistance term of porous media has a significant influence on pressure drop. Heat transfer coefficient and effective heat conductivity has a significant influence on temperature distribution. Calculation results from GATH are compared with a commercial CFD code named FLUENT. Good agreement between the two codes indicates the adopted methods in GATH are rational. GATH can be employed for thermal-hydraulic analysis of PB-FHRs.

KEYWORDS
PB-FHR, porous media, SIMPLEC algorithm, thermal dispersion, GATH

* Corresponding author.

1. INTRODUCTION

Pebble bed fluoride-salt cooled high temperature reactors (PB-FHRs) are Generation IV reactors which use coated particle pebble fuels and liquid fluoride-salt coolants. Coated particle pebble fuels, originally used in helium-cooled high temperature reactors, are spherical fuels that pile in the reactor core with the potential of on-line refueling via flow of the spheres through the core. In comparison with conventional reactor coolants, fluoride salt coolants have quite high volumetric heat capacities with high melting points and boiling points. Benefiting from the coated particle pebble fuels and liquid fluoride-salt coolants, PB-FHRs can operate under the condition of high temperature and low pressure with the potential of achieving excellent economic and safety performance[1].Attracted by the advanced design concept, several academic institutions around the world are concentrating on further study of PB-FHRs. University of California, Berkeley (UCB) developed a modular PB-FHR design in 2008 and an annular core type PB-FHR design in 2009[2, 3]. Shanghai Institute of Applied Physics, Chinese Academy of Sciences are designing a test reactor of PB-FHRs (named TMSR-SF) with the plan for its construction[4].

Thermal-hydraulics analysis for PB-FHRs is significant for both design and safety issues. Key thermal hydraulic phenomena in PB-FHRs include high Prandtl number of coolants, porous media flow of reactor core, freezing of coolants, radiant heat exchange, etc[5]. Porous media flow of reactor core is the research emphasis in this paper. Because of the tortuous flow paths formed by piled pebble fuels, intense heat convection occurs between fuels and coolant. Local coolants are sufficiently mixed in the tortuous flow paths, resulting in enhanced thermal dispersion. While thermal hydraulic codes for PB-FHRs are under development, some existing thermal hydraulic codes, which were successfully applied in other reactors before, have been modified for thermal hydraulic analysis of PB-FHRs. THERMIX, developed for high temperature gas cooled reactor (HTGR), were modified by De Zwaan et al. to calculate the fuel temperature distribution of PB-FHRs at the steady state operation[6]. UCB's reactor safety and mechanical design (RSMD) group employed COMSOL, which was a commercial multi-physics code including computational fluid dynamics (CFD) module, to simulate the flow distribution and pressure drop in the PB-FHR core by adding fluoride-salt properties [3]. Likewise, researchers of UCB embedded fluoride-salt properties and related correlations into RELAP5-3D, which was a system analysis code based on lumped parameter method and was widely used for transient analysis in light water reactors, to simulate the steady state operation and transient accidents for PB-FHRs[7].

The above modified codes have the modeling capability to analyze the thermal hydraulic phenomena in PB-FHR core, but several problems also exist in them. The momentum equations in THERMIX is simplified as quasi-static equations[8], so it is uncertain whether the calculated flow distribution and pressure drop are accurate enough for high-viscosity fluoride salt. Thermal dispersion mechanism in reactor core is considered by building the effective heat conductivity correlation of coolant in THERMIX, but this effective heat conductivity correlation is an empirical formula for high speed helium. So it is not clear whether the effective heat conductivity correlation of coolant in THERMIX can appropriately emerge the thermal dispersion mechanism for fluoride salt. COMSOL or other commercial CFD codes can provide quite fine analysis results, but they are difficult to be modified and time-consuming because of their closed-source and fine-modeling characteristics. RELAP5-3D, as a lumped-parameter code, uses more simplified mathematical models than THERMIX, so it also can not provide accurate and fine results for PB-FHR's core. Considering the exist problems, it is very essential and important to develop a specialized thermal-hydraulic code of reactor core for PB-FHR.

Aim of this study is to develop a fast running thermal-hydraulic code (named GATH) based on modern computational fluid dynamics (CFD) method for PB-FHRs to analyze detailed thermal-hydraulic phenomena in reactor core. Porous media model is applied to simplify reactor geometry. Energy equations for solid region and fluid region are constructed respectively with considering local thermal non-equilibrium effect between fuels and coolants. Two Energy equations are coupled by heat convection

terms in them. Macroscopic mass and momentum equations are solved to get speed distribution and pressure drop of coolants by using SIMPLEC (consistent semi-implicit method for pressure linked equations) algorithm. In order to give a more accurate depiction of thermal-hydraulics phenomenon of pebble bed, the thermal dispersion mechanism in the pebble bed is considered by solving modified macroscopic turbulence equations with additional source terms. Empirical correlations are used to calculate effective heat conductivity of pebble bed, resistance terms in momentum equations and heat transfer coefficient of coolants. Finite volume method is used for spatial discretization and fully implicit method for temporal discretization.

In this paper, mathematical models and numerical computation methods of GATH are described. GATH code is applied to analyze thermal hydraulic phenomena in a simplified PB-FHR model (a fuel channel assembly of modular PB-FHR) at steady state. Results by using different empirical correlations are compared to analyze the influences of effective heat conductivity, resistance terms and heat transfer coefficient. Calculation results from GATH are compared with those from a commercial CFD code (FLUENT) to validate the correctness of results and rationality of adopted methods.

2. MATHEMATICAL MODELS

Mathematical models in GATH are based on the turbulent heat transfer theory of porous media[9]. The complex geometry of pebble bed is treated as homogeneous media including a solid phase and liquid phase. The solid phase represents fuels in reactor core and the liquid phase represents fluoride-salt coolants. By means of volume-average method, basic conservation equations of the solid phase and liquid phase are constructed in macroscopic level.

2.1. The conservation equations of liquid phase

The conservation equations of liquid phase include the macroscopic mass, momentum, turbulent kinetic energy, turbulent dissipation rate and energy equation. Detail expressions and meanings of these equations are described below.

2.1.1. Macroscopic mass conservation equation of liquid phase

Fluoride-salt coolants are considered as incompressible fluid, mass conservation equation for liquid phase is written below:

$$\nabla \cdot \left(\phi \rho_f \boldsymbol{u} \right) = 0 \tag{1}$$

where ϕ is the porosity of porous media (the volume fraction of liquid phase), ρ_f is the density of liquid phase, $\boldsymbol{u}$ is the physical velocity of liquid.

2.1.2. Macroscopic momentum conservation equation of liquid phase

Macroscopic momentum conservation equation based on physical velocity is constructed to get flow distribution in reactor core. The equation is deduced from the microscopic Reynolds averaged momentum equations by applying volume-average method[10]. A resistance term caused by solid phase is added in the equation. Macroscopic momentum conservation equation can be written as

$$\phi \rho_f \frac{\partial u_i}{\partial t} + \frac{\partial}{\partial x_j}(\phi \rho_f u_i u_j) = -\frac{\partial}{\partial x_i}(\phi p + \frac{2}{3}\phi \rho_f k) + \frac{\partial}{\partial x_j}[\phi(\mu + \mu_t)(S_{ij} + S_{ji})] - \phi R_i - \phi \rho_f g_i \tag{2}$$

where

$$S_{ij} = \frac{1}{2}\left(\frac{\partial u_i}{\partial x_j} + \frac{\partial u_j}{\partial x_i}\right) \tag{3}$$

represents the macroscopic Reynolds stress tensor. u_i, R_i, g_i represents the component of velocity, resistance term and gravitational acceleration in the i direction. p, μ, k, μ_t represents pressure, viscosity, macroscopic turbulent kinetic energy and turbulent viscosity. The express of μ_t is similar to that of clear fluid flow, given by

$$\mu_t = \rho_f c_\mu \frac{k^2}{\varepsilon} \tag{4}$$

where $c_\mu = 0.09$ is a dimensionless constant related to the turbulence model, ε is the macroscopic dissipation rate. k, ε and μ_t only exist in turbulent flow regime ($Re_P > 300$) and can be obtained by solving macroscopic turbulent kinetic energy and dissipation rate equations. $Re_p = \phi\rho_f|\boldsymbol{u}|d_p/\mu$ is the Reynolds number based on the fuel diameter and d_p is the fuel diameter.

Because of lacking specialized empirical correlations for fluoride salt, R_i can be obtained from empirical correlations successfully applied in other fields. Ergun equation[11], which is widely used in packed bed reactors, is adopted in this paper. In order to analyze the influence of different resistance terms, KTA correlation[12], which is used in HTGR, is also used in this study.

2.1.3. Macroscopic energy equation of liquid phase

Temperature difference exists between fuels and coolants, so local thermal non-equilibrium effect is considered. Energy equations for solid phase and liquid phase should be constructed respectively and coupled through heat transfer terms[13]. For getting the coolant temperature, the energy equation for liquid phase is solved. The energy equation for liquid phase can be written as

$$\phi\rho_f c_{p_f}\frac{\partial T_f}{\partial t} + \rho_f c_{p_f}\nabla\cdot(\phi\boldsymbol{u}T_f) = \nabla\cdot[\lambda_{f,eff}\nabla T_f)] + ha(T_s - T_f) \tag{5}$$

where c_{pf}, T_f, $\lambda_{f,eff}$ and h denote the heat capacity at constant-pressure, temperature, effective thermal conductivity and heat transfer coefficient of liquid phase. $a = 6(1-\phi)/d_p$ denotes the solid surface area per unit volume.

$\lambda_{f,eff}$ accounts for the stagnant heat conductivity of the liquid phase and the thermal dispersion effect due to fluctuations of microscopic velocity and temperature[14], which is given by

$$\lambda_{f,eff} = \phi\lambda_f + \lambda_{disp,m} + \lambda_t + \lambda_{disp,t} \tag{6}$$

where λ_f is the stagnant heat conductivity of the liquid phase, $\lambda_{disp,m}$ is the mechanical thermal dispersion caused by the spatial deviations of microscopic time mean velocity and temperature, λ_t is the turbulent heat conductivity caused by time fluctuations of the macroscopic velocity and temperature, $\lambda_{disp,t}$ is the turbulent thermal dispersion caused by both time fluctuations and the spatial deviations of microscopic velocity and temperature.

Thermal dispersion is an important heat transfer mechanism for liquid phase in the transverse direction, which has a great influence on the radial temperature distribution of the reactor core. Kuwahara and Nakayama obtained the correlations of $\lambda_{disp,m}$ according to the microscopic results from the numerical study of different fluids flowing through an array of square rods[15]. The correlations were compared with the experimental data for packed beds and the results showed good agreements. The quite close results indicated that the correlations could be applied in PB-FHRs. Thus, the correlations of $\lambda_{disp,m}$ proposed by Kuwahara and Nakayama are adopted in this paper.

λ_t and $\lambda_{disp,t}$ only exist in the turbulent flow regime, but as important as $\lambda_{disp,m}$ and can not be neglected. As proposed by Marcelo S.J de Lemos[16], the sum of λ_t and $\lambda_{disp,t}$ can be obtained through the eddy diffusivity concept, written as

$$\lambda_t + \lambda_{disp,t} = \phi c_{p_f} \frac{\mu_t}{\sigma_T} \tag{7}$$

where $\sigma_T = 0.9$ is the turbulence Prandtl constant.

For the purpose of analyzing the influence of different effective thermal conductivities, the empirical correlation used in HTGR[8] is also adopted in this paper. This correlation accounts for the thermal dispersion mechanism of gas in the pebble bed and has been validated by experiment data[17].

The heat transfer term of liquid phase, $ha(T_s-T_f)$, represents the energy obtained from the solid phase. The heat transfer correlation proposed by Wakao[18], which is applicative for packed beds in the Re range from 15 to 8500, is adopted in this paper. The KTA heat transfer correlation used in HTGR[19] is also adopted for comparison calculation.

2.1.4. Macroscopic turbulent kinetic energy and dissipation rate equation of liquid phase

In the turbulent flow regime, turbulent viscosity μ_t and the sum of λ_t and $\lambda_{disp,t}$ must be determined before solving the momentum equation (2) and the energy equation (7). According to equation (4) and (11), the values of μ_t and $\lambda_t + \lambda_{disp,t}$ are determined by the macroscopic turbulent kinetic energy and dissipation rate. Thus, the macroscopic turbulent kinetic energy and dissipation rate equation are solved in this paper. Guo et al.[20] applied three typical turbulence models to a pebble bed and pointed out the turbulence model of Nakayama and Kuwahara could give the most reasonable turbulent viscosity. Thus, the macroscopic turbulence model proposed by Nakayama and Kuwahara[10] is adopted, given by

$$\phi\rho_f \frac{\partial k}{\partial t} + \frac{\partial}{\partial x_j}(\phi\rho_f u_j k) = \frac{\partial}{\partial x_j}[(\mu + \frac{\mu_t}{\sigma_k})\frac{\partial \phi k}{\partial x_j}] + 2\phi\mu_t S_{ij} S_{ij} - \phi\rho_f \varepsilon + \phi\rho_f S_k \tag{8}$$

$$\phi\rho_f \frac{\partial \varepsilon}{\partial t} + \frac{\partial}{\partial x_j}(\phi\rho_f u_j \varepsilon) = \frac{\partial}{\partial x_j}[(\mu + \frac{\mu_t}{\sigma_\varepsilon})\frac{\partial \phi\varepsilon}{\partial x_j}] + \phi(2c_1\mu_t S_{ij} S_{ij} - c_2\rho_f \varepsilon)\frac{\varepsilon}{k} + \phi\rho_f S_\varepsilon \tag{9}$$

Where the additional source terms

$$S_k = 39\phi^2(1-\phi)^{5/2}\frac{(u_j u_j)^{3/2}}{d_p} \tag{10}$$

and

$$S_\varepsilon = c_2 \frac{S_k^2}{3.7\phi^{3/2}(1-\phi)(u_j u_j)} \tag{11}$$

represent the production of kinetic energy and dissipation rate due to the microscopic structure of porous media. k and ε represent the kinetic energy and dissipation rate. c_1=1.44, c_2=1.92, σ_k = 1.00 and σ_ε= 1.3 represent the dimensionless constants related to the turbulence model.

2.2. The conservation equation of solid phase

The conservation equation of solid phase is macroscopic heat conduction equation. Solid phase is considered fixed in the reactor. Macroscopic heat conduction equation is constructed to calculate temperature distribution of solid phase.

$$(1-\phi)\rho_s c_{ps} \frac{\partial T_s}{\partial t} = \nabla \cdot (\lambda_{s,eff} \nabla T_s) + q_n - ha(T_s - T_f) \tag{12}$$

where ρ_s, c_{ps}, T_s and $\lambda_{s,eff}$ denote the density, heat capacity at constant-pressure, temperature and effective thermal conductivity of solid phase. q_n is the nuclear heat source provided by neutronic codes . The heat transfer term exists as a cooling source related with the temperature of liquid phase.

The effective thermal conductivity of solid phase is given by the Zehner-Bauer-Schlünder (ZBS) correlation which is widely used in pebble bed reactors. The ZBS correlation takes account of all heat transfer mechanisms except heat convection, as written below:

$$\lambda_{s,eff} = \lambda_{s,cont} + \lambda_{s,f} + \lambda_{s,rad} \tag{13}$$

where $\lambda_{s,cont}$ accounts for the heat conduction through contact of pebbles, $\lambda_{s,f}$ accounts for the heat conduction through the liquids in the voids, $\lambda_{s,rad}$ accounts for the heat radiation among pebbles. The detail expression of ZBS correlation is described in [21].

3. NUMERICAL COMPUTATION METHODS

3.1. Discretization method

The conservation equations of physics variable (velocity, pressure, temperature, etc) in section 2 can be written as a general form

$$\phi\rho \frac{\partial \psi}{\partial t} + \rho\nabla \cdot (\phi \boldsymbol{u}\psi) = \nabla \cdot [\Gamma \cdot \nabla \psi)] + S \tag{14}$$

where Ψ represents the physics variable, Γ represents the general diffusion coefficient and S represents the general source term. The general conservation equation consists of a temporal term, convection term, diffusion term and source term.

Finite volume method is used for spatial discretization in 2D cylindrical coordinate and fully implicit method for temporal discretization. The staggered grid technology is employed, meaning velocity is stored on the faces of control volumes and other variables (pressure, temperature, etc) is stored in the center of control volumes. The first-order upwind difference method is used for the convection term and

the first-order backward difference method for the temporal term. By integrating the general conservation equation over each control volume, the general discretization equation is obtained, written as

$$a_P\psi_P = a_E\psi_E + a_W\psi_W + a_N\psi_N + a_S\psi_S + b \tag{15}$$

where a_P, a_E, a_W, a_N, a_S are coefficients for the unknown variables on the center, east, west, north and south of the control volume. b is the coefficient about the source term.

All the discretization equations in the calculation domain form an algebraic equation set with a five-diagonal coefficient matrix. The algebraic equation set is solved by biconjugate gradient stabilized method. These coefficients depend on the unknown variables, so the discretization equations are nonlinear and need to be solved iteratively, updating coefficients at each iteration until convergence.

3.2. SIMPLEC algorithm

The macroscopic momentum equation can not be solved directly due to the coupling of velocity and pressure. The SIMPLE-like algorithms such as SIMPLE, SIMPLER, SIMPLEC, etc. which are based on the pressure correction method, have been extensively used to deal with this coupling problem. Compared with other SIMPLE-like algorithms, the SIMPLEC (consistent semi-implicit method for pressure linked equations) algorithm[22] introduces less approximation and has better robustness. Thus, the SIMPLEC algorithm is adopted in this paper to calculate the velocity and pressure of coolants.

According to the SIMPLEC algorithm, the velocity is calculated with an assumed pressure firstly. The velocity and pressure correction values are calculated by solving the pressure correction equation. Then the calculated velocity and pressure are corrected by adding the correction values. The relationship between the velocity and pressure correction values is written as

$$(a_e - \sum a_{nb})u_e^{'} = A_e(P_P^{'} - P_E^{'}) \tag{16}$$

where a_e and a_{nb} are coefficients, $u^{'}_e$ is the velocity on the east face of control volume, A_e is the area of the east face, $P^{'}_p$ and $P^{'}_E$ are the pressure correction values on the center and east of control volume.

Based on the equation (23) and the mass conservation equation (1), the pressure correction equation is derived as a similar form to equation (22), given by

$$a_P P_P^{'} = a_E P_E^{'} + a_W P_W^{'} + a_N P_N^{'} + a_S P_S^{'} + b \tag{17}$$

Combined with the SIMPLEC algorithm, the solution procedure of GATH code can be summarized as

1. Initialize the physics variables and thermophysical properties of each phase.
2. Calculate the velocity in the radial and axial direction by solving equation (2).
3. Calculate the pressure correction values by solving equation (24).
4. Correct the velocity and pressure values.
5. Calculate the turbulent kinetic energy and turbulent dissipation rate by solving equation (15) and (16).
6. Calculate the temperature of coolants and fuels by solving equation (7) and (19).
7. Update the thermophysical properties according to the above results and return to step 2. The loop will not end until all the physics variables are convergent.
8. For transient calculation, return to step 2 and start the calculation for next time step until the last time step. For steady state calculation, end the calculation.

4. THERMAL HYDRAULIC ANALYSIS OF PB-FHRs

4.1. Description of the simplified PB-FHR model

The simplified PB-FHR model analyzed in this paper is shown in figure 1, which is a cylindrical pebble fuel channel in the modular PB-FHRs. Main design parameters of this model has been given by reference[23]. The reactor core of modular PB-FHRs includes seven fuel assemblies and each assembly consists of 19 pebble fuel channels. The height of pebble fuel channel is 3.2 m and the diameter is 0.198 m. The diameter of pebble fuels filled in the channel is 0.03 m. FLiBe is used as coolants, flowing through the channel from the bottom to the top. The porosities near the wall is larger than those near the center. For considering the effect of uneven porosity distribution, the porosity is set as

$$\phi = \begin{cases} 0.3954, & r <= 0.075\ m \\ 0.5738, & r > 0.075\ m \end{cases} \tag{18}$$

where r is the coordinate in the radial direction.

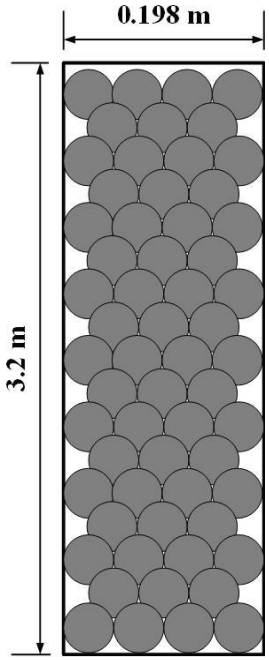

Figure 1. The pebble fuel channel in the modular PB-FHRs.

Under steady-state condition, the power of the reactor is 600MW_{th}. The mass flow rate of coolants is 6.2267 kg/s and the inlet temperature is 873.15 K. According to the results in reference[23], the nuclear power density (W/m^3) in the fuel channel is given by

$$q_n = \frac{6.0(1-\phi)}{\pi d_p^3}(-889.0z^2 + 2873.4z + 47.6) \tag{19}$$

where z is the coordinate in the axial direction.

4.2. Analysis for the steady state

The simplified PB-FHR model under the steady state is analyzed by GATH code. Spatial discretization is implemented in 2D cylindrical coordinate. Adiabatic boundary condition is applied on the wall. Heat transfer coefficient is calculated by Wakao correlation. Resistance terms is calculated by Ergun equation. The effective thermal conductivity of liquid phase is calculated by the macroscopic turbulence model.

Figure 2 shows the pressure and superficial speed distribution of coolants in the fuel channel. The pressure distributes uniformly along the radial direction and drops largely along the flowing direction. The total pressure drop excluding gravity is 19932.7 Pa. The superficial speed increases slightly along the axial direction. The coolants in the high-porosity regime flow faster than those in the low-porosity regime. The maximal speed is 0.1628 m/s, appearing at the outlet and the minimal speed is 0.0704 m/s, appearing at the inlet.

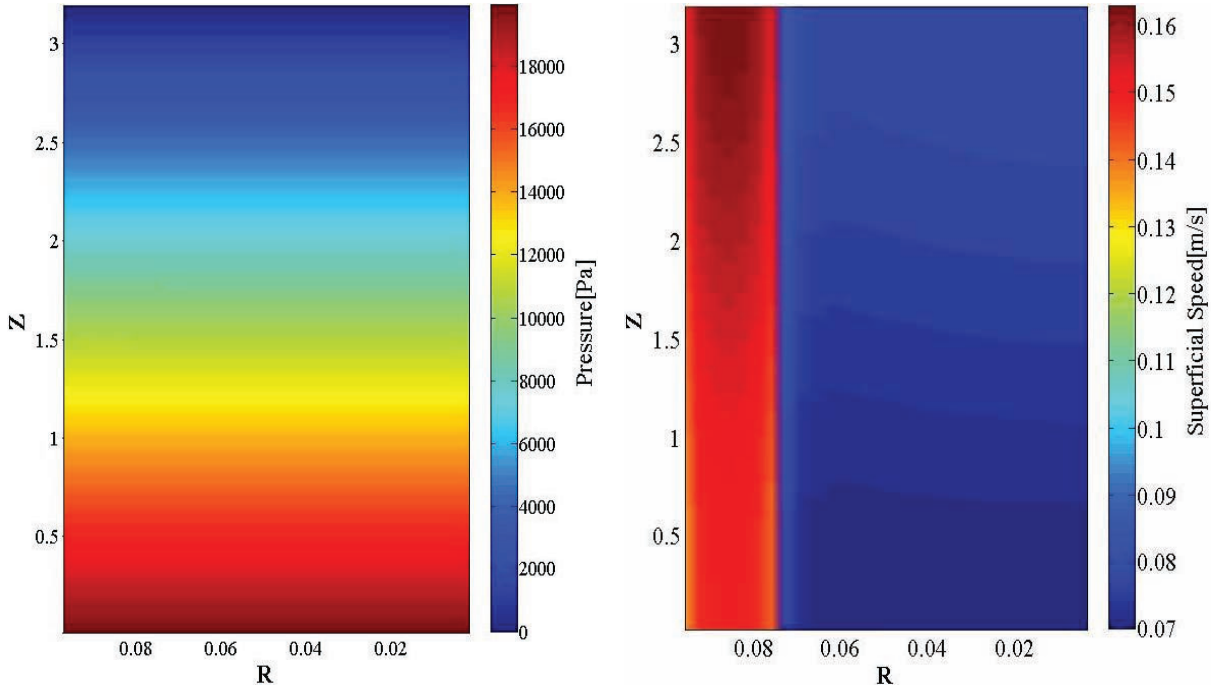

Figure 2. The pressure (left) and superficial speed (right) distribution of coolants.

Figure 3 shows the temperature distribution of coolants and fuels. The coolants temperature increases along the axial direction and decreases gradually along the radial direction. The highest temperature of coolants is 1270.9 K, appearing at the radial center and close to the outlet and the lowest temperature of coolants is 873.2 K, appearing at the inlet.

The fuels temperature is relatively higher than the coolants temperature at the same position. It decreases faster along the radial direction compared with the coolants temperature. The temperature in the high-porosity regime is higher than that in the low-porosity regime. The fuels temperature increases along the axial direction below Z = 2.5 m and then decreases. The highest temperature of fuels is 1337.5 K, appearing at the radial center and Z = 2.5 m and the lowest temperature of fuels is 879.8 K, appearing at the inlet.

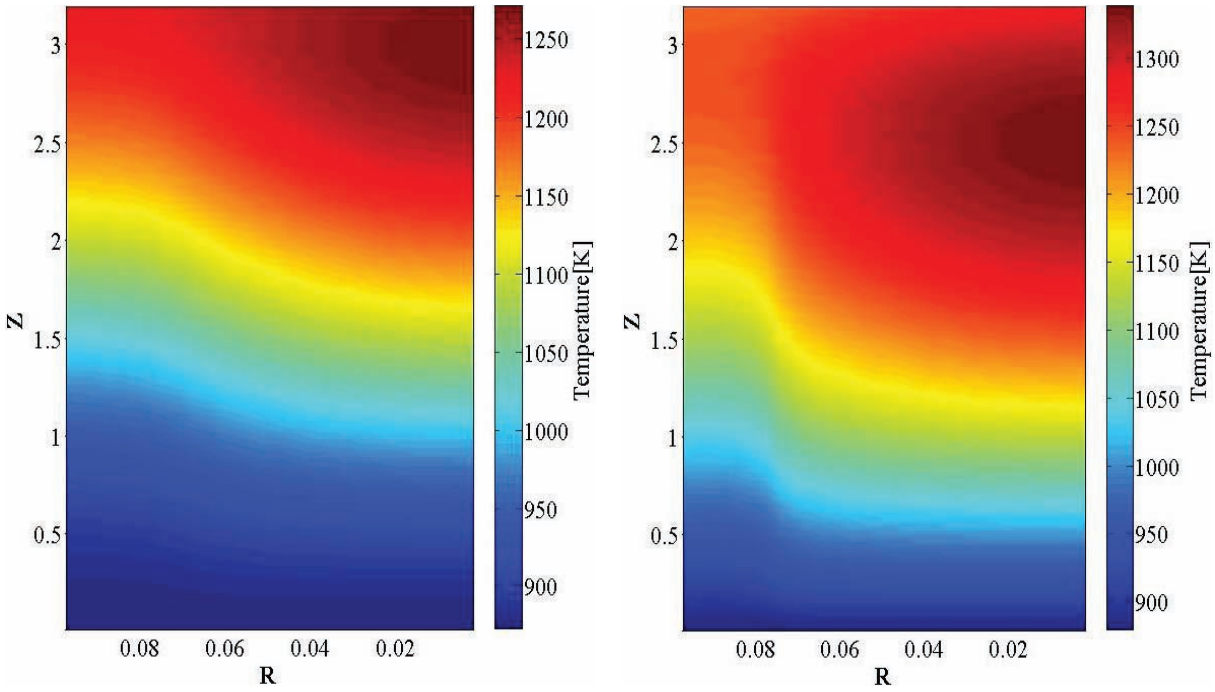

Figure 3. The temperature distribution of coolants (left) and fuels (right).

4.3. Influences of different correlations

As mentioned in section 2, specialized empirical correlations for PB-FHRs are lacking. Some existing empirical correlations have the potential to be applied in PB-FHRs, but influences of different correlations on analysis results is unclear. Thus, key results obtained by using different correlations are compared in this section to analyze the influences of different correlations.

Table I shows the results obtained with different effective liquid heat conductivities. λ_{center} is the effective liquid heat conductivity in the model center. $T_{f,\,max}$ is the maximal coolants temperature. $T_{f,\,mean}$ is the mean coolants temperature. $T_{s,\,max}$ is the maximal fuels temperature. $T_{s,\,mean}$ is the mean fuels temperature. ΔP is the pressure drop. U_{center} is the coolants speed in the model center. λ_{center} calculated by the HTR empirical correlation is larger than that calculated by the macroscopic turbulence model, resulting in lower $T_{f,\,max}$ and $T_{s,\,max}$. The effective liquid heat conductivity has slight influences on $T_{f,\,mean}$, $T_{s,\,mean}$, ΔP and U_{center}.

Table I. Results obtained with different effective liquid heat conductivities

Results	λ_{center} / W·m·K^{-1}	$T_{f,\,max}$ /K	$T_{f,\,mean}$/K	$T_{s,\,max}$ /K	$T_{s,\,mean}$ /K	ΔP /Pa	U_{center} /m·s^{-1}
$\lambda_{f,eff}$	590.7	1270.9	1049.4	1337.5	1154.9	19932.7	0.0747
$\lambda_{f,HTGR}$	839.8	1255.2	1048.7	1320.3	1152.9	20065.1	0.0747

Table II shows the results obtained with different resistance terms. R_{center} is the resistance term in the model center. R_{center} calculated by the KTA empirical correlation is smaller than that calculated by the Ergun empirical correlation, resulting in lower ΔP and U_{center}. The temperature of coolants and fuels increase slightly due to the decrease of U_{center}.

Table II. Results obtained with different resistance terms

Results	R_{center} /Pa·m^{-1}	$T_{f,\,max}$ /K	$T_{f,\,mean}$/K	$T_{s,\,max}$ /K	$T_{s,\,mean}$ /K	ΔP /Pa	U_{center} /m·s^{-1}
R_{ergun}	2456.2	1270.9	1049.4	1337.5	1154.9	19932.7	0.0747
R_{KTA}	1923.5	1273.8	1049.9	1342.2	1156.3	15674.0	0.0731

Table III shows the results obtained with different heat transfer correlations. h_{center} is the heat transfer coefficient in the model center. h_{center} calculated by the KTA empirical correlation is larger than that calculated by the Wakao correlation, resulting in lower $T_{s,\,max}$ and $T_{s,\,mean}$. The heat transfer correlation has slight influences on $T_{f,\,max}$, $T_{f,\,mean}$, ΔP and U_{center}.

Table III. Results obtained with different heat transfer correlations

Results	h_{center} /W·m^{-2}·K^{-1}	$T_{f,\,max}$ /K	$T_{f,\,mean}$/K	$T_{s,\,max}$ /K	$T_{s,\,mean}$ /K	ΔP /Pa	U_{center} /m·s^{-1}
Nu_{Wakao}	5308.5	1270.9	1049.4	1337.5	1154.9	19932.7	0.0747
Nu_{KTA}	7134.1	1271.1	1049.4	1317.4	1139.1	19932.6	0.0747

4.4. Comparison with FLUENT code

For validating the accuracy of GATH code and rationality of adopted methods, the results in section 4.2 are compared with those from a commercial CFD code named FLUENT. A 3D model of PB-FHRs is adopted and meshed with unstructured grids in FLUENT. The results from the two codes (see figure 4, figure 5 and table IV) show good agreement.

Figure 4 shows the axial temperature distribution of coolants and fuels at R = 0 m obtained from the two codes. The maximum discrepancy of coolants temperature from the two codes is 19.2 K, appearing at Z = 1.26 m. The maximum discrepancy of fuels temperature is 17.5 K, appearing at Z = 1.71 m.

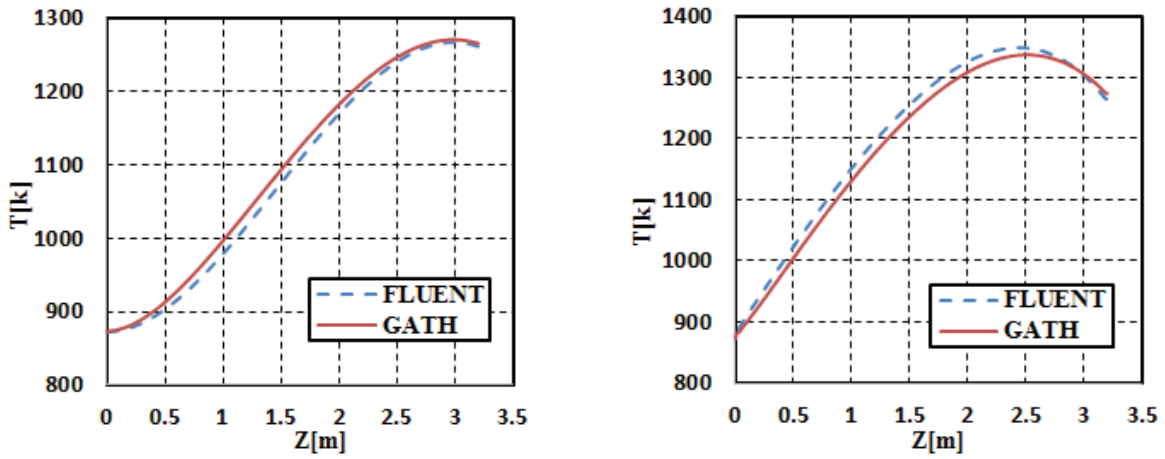

Figure 4. The axial temperature distribution of coolants (left) and fuels (right) at R = 0 m.

Figure 5 shows the radial temperature distribution of coolants and fuels at Z = 3.15 m obtained from the two codes. The maximum discrepancy of coolants temperature is 3.5 K, appearing at R = 0.099 m. The maximum discrepancy of fuels temperature is 7.5 K, appearing at R = 0 m.

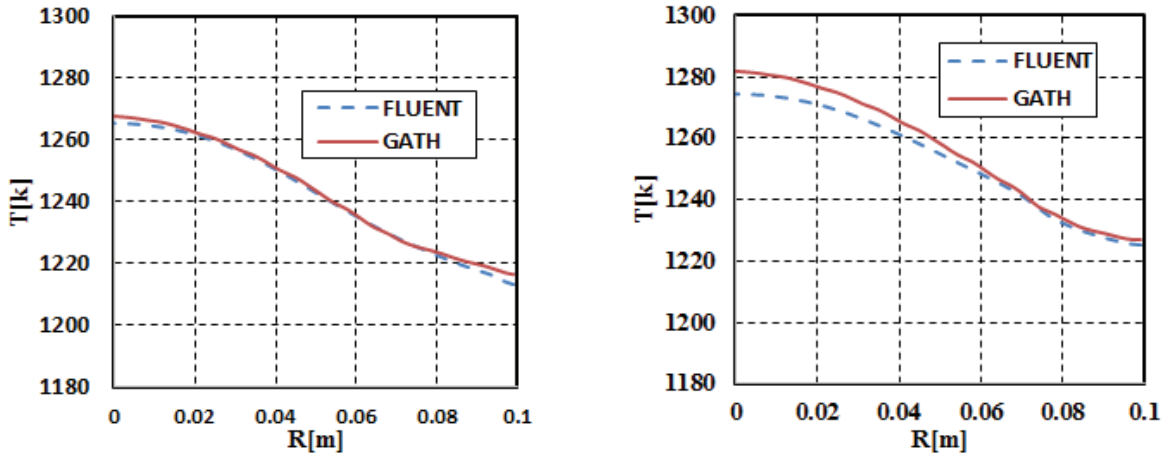

Figure 5. The radial temperature distribution of coolants (left) and fuels (right) at Z = 3.15 m.

Table IV shows the key results from the two codes. $T_{f,\,outlet}$ is the mean coolants temperature at the outlet. The deviation of $T_{f,\,outlet}$ is smallest among all the key results. All the deviations of results related to temperature are smaller than 1%. Both ΔP and U_{center} from GATH are slightly higher. The deviations of ΔP and U_{center} are close to 2%.

Table IV. Key Results from GATH and FLUENT

Results	$T_{f,\,outlet}$ /K	$T_{f,\,max}$ /K	$T_{f,\,mean}$/K	$T_{s,\,max}$ /K	$T_{s,\,mean}$ /K	ΔP /Pa	U_{center} /m·s^{-1}
FLUENT	1230.4	1266.2	1057.3	1348.7	1152.5	19547.9	0.0730
GATH	1232.6	1270.9	1049.4	1337.5	1154.9	19932.7	0.0747
Deviation	0.18%	0.37%	0.75%	0.83%	0.21%	1.97%	2.28%

4.5. Discussion

The analysis results for the steady state indicate the porosity distribution has great influences on the pressure, speed and temperature distribution. Large pressure drop occurs due to the resistance of porous media. Because the resistance in the high-porosity regime is higher than that in the low-porosity regime, some coolants in the high-porosity regime flow to the low-porosity regime. Thus the speed of coolants is higher in the low-porosity regime. According to the energy conservation law, the temperature of coolants is directly proportional to the power density and inversely proportional to the speed under steady state. So the temperature of coolants is lower in the high-porosity regime. The heat transfer coefficient is also directly proportional to the speed of coolants. Higher heat transfer coefficient helps decrease temperature difference between fuels and coolants. Thus the temperature of fuels is lower in the low-porosity regime.

The influences of different correlations on analysis results have been shown in section 4.3. Heat conduction is the dominating heat transport mechanism in the radial direction. Higher effective heat conductivity of coolants helps heat transport more efficiently along the radial direction, resulting in more

flat temperature distribution. Thus $T_{f,\,max}$ and $T_{s,\,max}$ will decrease if the effective heat conductivity of coolants increase. The resistance terms of porous media is the main cause of pressure drop. Thus Lower resistance terms cause lower pressure drop. Different pressure distribution then causes different speed distribution. The temperature of coolants is mainly determined by the power density of fuels under steady state, so it changes little by using different heat transfer correlations. However, higher heat transfer coefficient helps decrease temperature difference between fuels and coolants. Thus the temperature of fuels decreases with higher heat transfer coefficient.

The results from GATH show good agreement with those from FLUENT. It indicates the results from GATH are correct and the adopted methods in GATH are rational. Slight deviations exist between the two codes due to the differences in modeling methods. The FLUENT code adopts 3D model and unstructured-grid meshing. The detail discretization methods in FLUENT are also different from GATH.

5. CONCLUSIONS

In this paper, a specialized thermal-hydraulic code with porous media model and SIMPLEC algorithm is developed for PB-FHRs to analyze detailed thermal-hydraulic phenomena in the reactor core. The thermal dispersion mechanism in the pebble bed is considered by solving macroscopic turbulence equations.

The steady state of the simplified PB-FHR model is analyzed by GATH. The porosity distribution has great influences on the pressure, speed and temperature distribution. Large pressure drop occurs due to the resistance of porous media. The temperatures of coolants and fuels are both lower in the high-porosity regime where the speed of coolants is higher and the power density is lower.

The influences of different correlations on analysis results are analyzed. The results indicate that the effective heat conductivity has significant influences on both coolants and fuels temperature distribution. The resistance term of porous media has significant influences on pressure drop and speed of coolants. The heat transfer correlation has significant influences on fuel temperature distribution.

Calculation results from GATH are compared with those from the FLUENT code to validate the correctness of results and rationality of adopted methods. Good agreement between two codes indicates the results from GATH are correct and the adopted methods in GATH are rational.

GATH code can be employed for thermal-hydraulic analysis of PB-FHRs. By coupling GATH with neutronic and structural mechanics codes, integrated safety analysis for PB-FHRs can be implemented. However, adopted empirical correlations in GATH are not optimal. Specialized empirical correlations for PB-FHRs need to be studied. Validation of GATH through experiment data is also necessary in further work.

ACKNOWLEDGMENTS

This paper is supported by the "Strategic Priority Research Program" of the Chinese Academy of Sciences, (Grant No. XDA02010200), and Science and Technology Commission of Shanghai Municipality (Grant No. 11JC1414900).

REFERENCES

1. C.W. Forsberg, P.F. Peterson, and P.S. Pickard, “Molten-salt-cooled advanced high-temperature reactor for production of hydrogen and electricity,” *Nuclear Technology*. **144**(3), pp. 289-302 (2003).
2. “UC Berkeley TH Reports,” http://fhr.nuc.berkeley.edu/wp-content/uploads/2014/10/08-001-PB-AHTR-NE170-Design-Project-Rpt.pdf (2008).

3. "UC Berkeley TH Reports," http://fhr.nuc.berkeley.edu/wp-content/uploads/2014/10/09-001_NE-170_2009_PB-AHTR_Core_Design.pdf (2009).
4. J. Serp, et al., "The molten salt reactor (MSR) in generation IV: Overview and perspectives," *Progress in Nuclear Energy*. **77**, pp. 308-319 (2014).
5. "UC Berkeley TH Reports," http://fhr.nuc.berkeley.edu/wp-content/uploads/2013/08/12-002-FHR-Workshop-2-Report-Final.pdf (2013).
6. S. De Zwaan, et al., "Static design of a liquid-salt-cooled pebble bed reactor (LSPBR)," *Annals of Nuclear Energy*. **34**(1), pp. 83-92 (2007).
7. "UC Berkeley TH Reports," http://fhr.nuc.berkeley.edu/wp-content/uploads/2014/10/07-001_PB-AHTR_LOFC_Griveau.pdf (2007).
8. "Oak Ridge National Lab., TN (USA)," http://web.ornl.gov/info/reports/1986/3445600661013.pdf (1986).
9. M.J. de Lemos and M.H. Pedras, "Recent mathematical models for turbulent flow in saturated rigid porous media," *Journal of Fluids Engineering*. **123**(4), pp. 935-940 (2001).
10. A. Nakayama and F. Kuwahara, "A macroscopic turbulence model for flow in a porous medium," *Journal of fluids engineering*. **121**(2), pp. 427-433 (1999).
11. S. Ergun, "Fluid flow through packed columns," *Chemical engineering progress*. **48**(1952).
12. "Nuclear Safety Standards Commission," http://www.kta-gs.de/e/standards/3100/3102_3e.pdf (1981).
13. M. Quintard, M. Kaviany, and S. Whitaker, "Two-medium treatment of heat transfer in porous media: numerical results for effective properties," *Advances in Water resources*. **20**(2), pp. 77-94 (1997).
14. F.D. Rocamora and M.J. de Lemos, "Analysis of convective heat transfer for turbulent flow in saturated porous media," *International communications in heat and mass transfer*. **27**(6), pp. 825-834 (2000).
15. F. Kuwahara and A. Nakayama, "Numerical modelling of non-Darcy convective flow in a porous medium," *Heat transfer*. **4**, pp. 411-416 (1998).
16. M.J. de Lemos and E.J. Braga, "Modeling of turburlent natural convection in porous media," *International communications in heat and mass transfer*. **30**(5), pp. 615-624 (2003).
17. E. Achenbach, "Heat and flow characteristics of packed beds," *Experimental Thermal and Fluid Science*. **10**(1), pp. 17-27 (1995).
18. N. Wakao, S. Kaguei, and T. Funazkri, "Effect of fluid dispersion coefficients on particle-to-fluid heat transfer coefficients in packed beds: correlation of Nusselt numbers," *Chemical engineering science*. **34**(3), pp. 325-336 (1979).
19. "Nuclear Safety Standards Commission," http://www.kta-gs.de/e/standards/3100/3102_2e.pdf (1983).
20. B. Guo, et al., "Simulation of turbulent flow in a packed bed," *Chemical engineering & technology*. **29**(5), pp. 596-603 (2006).
21. "IAEA TECDOC," http://www-pub.iaea.org/MTCD/publications/PDF/te_1163_prn.pdf (2000).
22. J. Van Doormaal and G. Raithby, "Enhancements of the SIMPLE method for predicting incompressible fluid flows," *Numerical heat transfer*. **7**(2), pp. 147-163 (1984).
23. "The Ohio State University," http://etd.ohiolink.edu/!etd.send_file?accession=osu1238045558&disposition=inline (2009).